Drug Design, Development and Therapy

Dovepress
Taylor & Francis Group

Open Access Full Text Article

ORIGINAL RESEARCH

Cationic Liposome-Mediated Bcl-2 Gene Transfection in Bone Marrow Mesenchymal Stem Cells: A Novel Regenerative Approach for Spinal Cord Injury

Haitao Yuan[1,*], Xiaojun Feng[1,*], Kamran Hidayat Ullah[2], Bo Chu[1], Tianqi Wang[1], Xin Zhou[1], Jun Gu[1]

[1]Department of Orthopedics, Xishan People's Hospital Of Wuxi City, Wuxi, Jiangsu, 204105, People's Republic of China; [2]Department of Pharmacy, CECOS University of IT and Emerging Sciences, Peshawar, Pakistan

*These authors contributed equally to this work

Correspondence: Jun Gu, Email wxgujun@njmu.edu.cn

Objective: This study explored a novel therapy for spinal cord injury (SCI) using cationic liposomes to deliver the anti-apoptotic Bcl-2 gene into rat bone marrow mesenchymal stem cells (BMSCs), followed by transplantation into a rat SCI model to evaluate its potential in promoting neural regeneration and enhancing SCI therapy.

Methods: BMSCs were isolated and characterized for surface markers and differentiation potential, and transfected with Bcl-2 via cationic liposomes. A rat SCI model was established to assess the therapeutic effects of BMSCs and Bcl-2-BMSCs. Functional recovery was evaluated using the Basso, Beattie, and Bresnahan (BBB) scale and inclined plate test, while histopathology, Western blot, and real-time polymerase chain reaction (RT-PCR) analyses were performed to assess neural recovery. Nissl and myelin staining were used to evaluate neuronal and myelin recovery.

Results: Following successful characterization of BMSCs and the spherical cationic liposomes (105 ± 1.3 nm, 18.65 ± 1.37 mV zeta potential), optimal transfection conditions were identified. Bcl-2-transfected BMSCs expressed high levels of Bcl-2 with low toxicity. In addition, the SCI results showed significant improvements in the BBB and inclined plate scores of rats in the BMSCs and Bcl-2-BMSCs groups compared to the model group ($p< 0.01$). HE-stained samples demonstrated that the secretion of Bcl-2 and BMSCs plays a crucial role in SC repair. Western blot results revealed an upregulation of proteins associated with neural recovery (Bcl-2, β-tubulin3, MAP2, NF-200, MBP) and a downregulation of the glial scar-associated protein GFAP in both the BMSCs and Bcl-2-BMSCs groups. Furthermore, Nissl staining and myelin staining showed that both the BMSCs and Bcl-2-BMSCs groups exhibited enhanced neuronal survival, inhibition of demyelination, and significant myelin regeneration.

Conclusion: Transplantation of Bcl-2-transfected BMSCs represents a highly promising strategy that effectively promotes neural regeneration, inhibits scar formation, reduces demyelination, and enhances functional recovery, highlighting its potential for clinical translation.

Keywords: bone marrow stromal cells, Bcl-2, cationic liposomes, spinal cord injury

Introduction

Spinal cord (SC) injury (SCI) is caused by vertebral fractures or dislocations resulting in damage to the SC or cauda equina nerve. Central nervous system disorders can lead to severe disabilities or motor dysfunctions. SCI can also be triggered by secondary damage due to physical trauma, tumors, infections, or degenerative disc diseases.[1] The pathological process of traumatic SCI is complex with high rates of disability and mortality.[2–4] SCI involves both primary and secondary injuries, including neuronal function inhibition due to neuronal tissue loss,[5] suppression of neural development

Received: 3 January 2025
Accepted: 12 November 2025
Published: 19 November 2025

by glial scar formation,[6,7] and restricted SCI recovery because of the upregulation of inhibitory molecules.[8] To prevent further damage to the SC, therapeutic strategies currently employed by physicians for SCI treatment include early surgical intervention and methylprednisolone sodium succinate at high-dose.[9,10] Despite these therapeutic options, the recovery of neural function is still limited, with a significant impact on patients' daily lives, thereby making it imperative to find more effective treatments for SCI.

Cell transplantation is a promising treatment option for SCI.[11] Within the broader landscape of regenerative strategies for SCI, several emerging approaches are under active investigation. These include cell-derived exosomes, which mediate therapeutic effects via paracrine signaling but pose challenges for standardized production and controlled delivery;[12] biomaterial scaffolds that provide structural support yet may provoke foreign body responses or lack sufficient bioactivity;[13] and CRISPR-based gene editing, which enables precise genetic modification but is hampered by delivery inefficiency and safety concerns.[14] In contrast, non-viral vector-mediated gene delivery, particularly employing cationic liposomes, offers a compelling alternative due to its well-established safety profile, high transfection efficiency, and relative ease of large-scale production.[15] Transplantation of mesenchymal stem cells (MSCs) into SCI models has been shown to promote neuron survival and support axonal regeneration. However, the extent of integration and neuronal differentiation of transplanted cells remains a topic of ongoing investigation. Recent studies have provided evidence that while MSCs may not directly differentiate into neurons, they contribute to SCI repair through paracrine signaling, which supports neuronal survival and regeneration.[16] Tissue engineering research generally involves three key components: 1) stem cells, 2) growth factors necessary for cell survival, and 3) scaffold materials.[17] Stem cells represent a unique class of therapeutic agents.[18] For example, in 2011, Hearticellgram-AMI, a stem cell-based therapeutic drug, was officially approved in South Korea for the treatment of acute myocardial infarction.[19] In 2012, Prochymal, a stem cell drug, was approved for use in Canada.[20] In September 2016, an injectable solution of human dental pulp mesenchymal stem cells was the first dental-derived stem cell drug accepted for registration in China.[21,22]

Mesenchymal stem cells (MSCs) are adult cells that can differentiate into cartilage, bone, fat, tendon, ligament, and other tissues.[23,24] In view of their ability to highly proliferate, potentially differentiate in a multilineage fashion, exhibit paracrine effects, and have low immunogenicity, scientists usually utilize MSCs as seed cells in tissue engineering.[25–28] Currently, MSCs are derived from bone marrow, bone, dental pulp, fat, and umbilical cords.[29–31] Bone marrow stromal cells (BMSCs), derived from the bone marrow tissue, are the most common source of MSCs.[32] MSCs are widely investigated for neural repair owing to their trophic, immunomodulatory, and pro-regenerative properties. BMSCs are multipotent mesenchymal stromal cells with multilineage differentiation capacity, classically along the osteogenic, chondrogenic, and adipogenic lineages.[33–36] As seed cells, BMSCs exhibit diverse differentiation abilities including osteogenesis, chondrogenesis, adipogenesis, and myogenesis.[37,38] However, challenges remain regarding the low rates of survival and differentiation of BMSCs into neural cells after cell transplantation.[39] Moreover, it remains unclear whether BMSCs directly promote axonal regeneration or not. Therefore, these issues limit the application of BMSCs in SCI treatment.

The anti-apoptotic protein B-cell lymphoma-2 (Bcl-2) belongs to the integrin membrane protein family and has a molecular weight of 26 kDa.[40,41] Bcl-2 is localized in the mitochondria, endoplasmic reticulum, and nuclear membrane via its C-terminal transmembrane domain.[42] The mitochondrial apoptotic pathway is regulated primarily by the Bcl-2 protein family.[42,43] Bcl-2 binds to pro-apoptotic proteins and inhibits outer membrane permeability in mitochondria, thereby preventing cytochrome c release into the cytoplasm and inhibiting apoptosis.[44] In addition, Bcl-2 is involved in regulating neuronal differentiation,[45] which can be promoted by the overexpression of Bcl-2.[46,47] Through family of Bcl-2 protein, the neuronal cells regulate cell death and axonal degeneration.[48] Studies in rat brain ischemia models have shown that Bcl-2 overexpression promotes cortical neuron survival and substantially enhances the differentiation of transplanted stem cells from embryos into neurons,[15,49,50] thereby resulting in improved functional recovery. In addition to facilitating the regeneration of axons via the Ca^{2+}-ERK/CREB pathway, the anti-apoptotic protein Bcl-2 promotes the survival and differentiation of neural cells.[48,51] In addition, the overexpression of Bcl-2 is closely linked to the functionality of BMSCs.[15] Secondary injury in SCI is characterized by widespread apoptosis of host neurons and glia as well as poor survival of transplanted cells. Bcl-2 is a canonical anti-apoptotic regulator; transient overexpression can increase cell survival and preserve tissue integrity in acute CNS injury models. We therefore selected Bcl-2 to enhance

the survival and therapeutic activity of transplanted BMSCs. Prior reports similarly describe improved graft survival and functional benefit with Bcl-2-overexpressing stem cells in CNS contexts.[52,53]

In this study, Bcl-2 expression was achieved via non-viral plasmid transfection, minimizing integration risk. We used cationic liposomes, a non-viral platform that complexes DNA through electrostatic interactions. Compared with viral vectors, cationic liposomes offer straightforward preparation, low immunogenicity, and flexible dosing, while achieving practical transfection efficiency in MSCs with low cytotoxicity under optimized conditions. This approach balances efficacy and safety, aligning with our goal of transiently augmenting BMSC survival and function after SCI. Prior studies have reported that Bcl-2–overexpressing stem cells show improved survival and functional benefit in CNS injury models.[15,47,50,54]

This study aimed to investigate the effect of Bcl-2 overexpression on cell viability and analyze the impact of Bcl-2-overexpressing BMSCs on SCI repair in rats. This study aimed to provide new insights into optimizing BMSC transplantation strategies for SCI repair and offering theoretical and technical guidance for clinical SCI treatment.

Materials and Methods

Materials

Ethanol was supplied by Sinopharm Chemical Reagent Co. Ltd. Beijing Solarbio Science and Technology. Co., Ltd. provided kits for bicinchoninic acid (BCA) assay, cholesterol, hematoxylin-eosin staining, 3-(4, 5-dimethyl-thiazolyl-2)-2, 5-diphenyl-tetrazolium bromide (MTT) assay, phosphate-buffered saline (PBS), formaldehyde, and 3% phosphotungstic acid solution. The Nissl staining kit, Sirius Red staining solution, Oil Red O staining, and Luxol Fast Blue Myelin Staining Kit were obtained from Shanghai Zeyebio Biotechnology Co., Ltd. Fetal bovine serum (FBS), Dulbecco's modified Eagle medium (DMEM), and trypsin were purchased from Gibco. Antibodies against CD29 (11–0291-82), CD34 (11–0341-82) and CD90 (14–0909-82) were purchased from Thermo Fisher Scientific (USA). Antibodies against Bcl-2 (ab196495), β-tubulin 3 (ab18207), microtubule-associated protein-2 (MAP2, ab5392), glial fibrillary acidic protein (GFAP, ab7260), nestin (ab221660), myelin basic protein (MBP, ab7349) and β-actin (ab8226) were purchased from Abcam (USA). Anti-neurofilament (NF-200, #55453) antibody was purchased from CST (USA). The pre-stained colored protein marker (BP107) was purchased from Bio-Platform (Guangzhou, China). The NH OsteoDiff Medium was purchased from Miltenyi Biotec (Germany).

Isolation and Identification of Rat BMSCs

Sprague-Dawley (SD) rats with a mean weight of approximately 250 g were purchased from Charles River (Beijing, China). All animal procedures were performed in accordance with a protocol approved by the Ethics Committee of Xishan People's Hospital Of Wuxi City (approval number: xs2020ky015). In addition, we strictly adhered to the ethical guidelines outlined in the *Guide for the Care and Use of Laboratory Animals* to ensure proper animal welfare throughout the study. After ensuring proper care of the rats in conducive laboratory environments, they were anesthetized and sacrificed via dislocation of the cervical spine before their skin was disinfected with 75% ethanol, as reported in other studies,[55,56] with some modifications. The skin and muscles around the femurs and tibias were quickly cut open under sterile conditions, and bones were extracted and soaked in PBS. The bones were disinfected under ultraviolet light for 30 min and washed thrice with PBS containing penicillin and streptomycin. Both ends of the bone were removed to expose the bone marrow cavity. Under aseptic conditions, a 5-mL sterile syringe fitted with an 18-gauge (18G) needle was used to inject 5 mL of growth medium through one end of the bone to flush the marrow, which was collected in a sterile Petri dish.

The cell suspension was aspirated and resuspended to disperse the cells, and then collected in a 15 mL centrifuge tube. The sample was centrifuged at 1000 rpm for 5 min at room temperature. The supernatant was discarded, and the pellet was resuspended in 6 mL of complete medium. The single-cell suspension was transferred to a culture dish and incubated. After 24 h, the cells were observed under a microscope; most were spherical and composed of red blood cells. The medium was then replaced to remove floating blood cells. Subsequently, the medium was changed every 2–3 days until the cells reached 80–90% confluency, at which point they were passaged.

BMSC identification was performed according to the available protocol with slight modifications.[56] The third passage (P3) of BMSCs was harvested by trypsinization. Cells were resuspended in PBS at a concentration of 1×10^6/mL. Flow cytometry was performed using antibodies against CD29, CD34, and CD90, with three parallel samples for each antibody, every single sample represents an independent experimental case. Immunofluorescence staining was performed using the anti-CD29, anti-CD34, and anti-CD90 antibodies. For qualitative marker assessment only, COL2A1 immunofluorescence was carried out on baseline cultures (no induction) using anti-type II collagen antibody. Before blocking the membranes with goat serum and permeabilization with 0.1% Triton X-100, cells were fixed for 15 min in paraformaldehyde (PFA, 4%). The samples were incubated with primary antibodies overnight at 4 °C, and with fluorescent secondary antibodies at room temperature for 30 min. Fluorescence microscopy was used to observe the protein expression levels.

To assess differentiation potential, cells were induced to differentiate into osteoblasts and adipocytes, as described previously.[57] For osteogenic differentiation, cells were seeded in 6-well plates at a density of 5×10^4 cells/well and cultured in osteogenic induction medium. After 10 days, the cells were fixed with 95% ethanol and stained with Alizarin Red. For adipogenic differentiation, cells were induced with high-glucose medium containing 5 μg/mL insulin, 0.5 mmol/L IBMX (3-isobutyl-1-methylxanthine), and dexamethasone (1 μmol/L). After 4 days, Oil Red O staining was performed to visualize lipid droplets. For chondrogenic differentiation, cells were centrifuged to form micromasses at a density of 2.5×10^5 cells/tube and cultured in chondrogenic induction medium containing 1% ITS+ Supplement, 50 μg/mL ascorbic acid, 100 nM dexamethasone, and 10 ng/mL TGF-β3. After 21 days, the chondrogenic pellets were fixed with 4% paraformaldehyde and stained with Toluidine blue to detect proteoglycan synthesis.

Preparation of Bcl-2 Gene-Loaded Cationic Liposomes

Preparation of Blank Cationic Liposomes

Based on Bangham method,[58] a mixture of DSPC (80 μL, 1.0 mmol/L), DSPE-PEG (80 μL, 1.0 mmol/L), and cholesterol (25 μL, 1.0 mmol/L) was dissolved in 3 mL of chloroform. The solvent was evaporated under reduced pressure using a rotary evaporator to form a thin lipid film. The film was resuspended in 2 mL of either water or PBS and then extruded 20 times through a 0.45 μm polycarbonate membrane to obtain uniformly sized cationic liposomes.

Preparation of Bcl-2 Plasmid-Loaded Cationic Liposomes

Expression plasmid. We used a Bcl-2 expression plasmid comprising the rat Bcl-2 ORF cloned into pcDNA3.1 under the CMV immediate-early promoter (Kozak consensus upstream of ATG; vector-encoded 3′ polyadenylation signal). The coding sequence corresponds to GenBank: L14680.1. The plasmid was constructed and synthesized by GenScript (Nanjing, China), amplified in E. coli, and purified using an endotoxin-free maxiprep; insert identity and orientation were confirmed by Sanger sequencing.

Lipoplex formation. For transfection,[59,60] 1 μg of the Bcl-2 expression plasmid was mixed with the cationic liposome formulation in serum-free medium to form DNA–lipid complexes (lipoplexes) at the indicated N/P ratio = 10:1. The mixture was gently combined and allowed to complex at room temperature before application to cells as described in Effect of Bcl-2 Plasmid-Loaded Cationic Liposomes on BMSCs Differentiation.

Characterization of Blank and Bcl-2 Plasmid-Loaded Cationic Liposomes

The cationic liposomes were diluted with water to a final volume of 10 mL. The diluted solution was added to the sample chamber for measurement, wherein the particle number served as the basis for determining particle size and zeta potential. Each sample was measured six times, and the average value was calculated, with each measurement taking 20s. In this study, each sample is the result of an individual and independent experiment. To determine the morphology, a particular quantity of cationic liposomes was diluted as described above, before an appropriate volume of the diluted solution was transferred to a small beaker. After allowing it to stand for 10 min, 3% phosphotungstic acid was added to ensure negative staining. The negative staining solution was then aspirated and dropped onto a copper grid, and excess staining solution was removed using filter paper. The sample was allowed to stand for 30 min to enable the particle deposition on the Cu grid. The size and morphology of the particles were observed by transmission electron microscopy

(TEM). All measurements were conducted at 25°C. Dynamic Light Scattering (DLS) was used to assess liposomal size, polydispersity index (PDI), and zeta potential of the formulation.

Effect of Bcl-2 Plasmid-Loaded Cationic Liposomes on BMSCs Differentiation

BMSCs (seeded at 1×10^5 cells/well in 6-well plates, 70% confluent) were exposed to 100 μg/mL Bcl-2-liposomes for 4 h, followed by medium replacement and further cultivation. The effect of transfection on cell viability was measured using the MTT assay.[61] BMSCs were incubated with varying concentrations of Blank-liposome and Bcl-2-liposome solutions (1, 5, 10, 50, 100, and 200 μg/mL). After 3 days of incubation, the MTT solution was added, and the absorbance was measured at 490 nm to calculate cell viability. Cell Viability (%) = $(OD_{\text{Experimental Group}}/OD_{\text{Negative Control Group}})\times 100$.

Bcl-2 expression was measured using an enzyme-linked immunosorbent assay kit (ELISA; Mlbio, Shanghai, China), and protein expression was detected by Western blotting. Protein samples were extracted from the cells and quantified using a BCA assay. Normality was assessed by Shapiro–Wilk and variance homogeneity by Levene's test. Because variances were unequal (Levene p=0.004), group differences in Bcl-2 expression were analyzed using Welch's one-way ANOVA, followed by Welch t-tests for pairwise comparisons with Bonferroni adjustment. We report two-sided exact p values. Effect sizes are η^2 for the omnibus test and Hedges' g for pairwise comparisons, each with 95% CIs.

Further, Proteins were separated by SDS-PAGE, transferred to a PVDF membrane, blocked with 5% non-fat milk, and incubated with anti-Bcl-2 primary antibody (1:100) at 4 °C overnight. After washing, the membrane was incubated with secondary antibody at room temperature for 60 min. Protein bands were visualized using ECL detection, and the relative expression levels were analyzed.

Cellular Uptake of Rhodamine B-Loaded Cationic Liposomes

Cationic liposomes were prepared by thin-film hydration as in Preparation of Bcl-2 Gene-Loaded Cationic Liposomes. Briefly, the dried lipid film was hydrated with PBS (pH 7.4) containing Rhodamine B (10 μg/mL), vortexed, and briefly sonicated. Liposomes were extruded sequentially through 0.45 μm and 0.20 μm polycarbonate membranes to obtain a uniform suspension. All steps involving dye were performed under low light. To eliminate unencapsulated Rhodamine B, the suspension was subjected to gel-filtration using Sephadex G-50, and the final retentate was brought to the desired lipid concentration. The absence of free dye was verified by measuring fluorescence in the filtrate versus the retentate.

MSCs were seeded at 5×10^5 cells/mL (2 mL/dish) in glass-bottom confocal dishes and cultured 24 h to ~60-70% confluence. Cells were then incubated with Rhodamine B-loaded liposomes (final 10 μg/mL, lipid-equivalent) in complete medium at 37 °C. Prior to imaging, cells were washed 3× with PBS to remove non-internalized material. Uptake was assessed by fluorescence microscopy at 24 h and 48 h using identical exposure/gain settings across all groups (Rhodamine B ex/em ~540/625 nm). Nuclei were counterstained with DAPI where indicated.

Effects of Bcl-2 Plasmid-Loaded Cationic Liposomes on Rats with SCI

Construction of Rat Model of SCI

The night before surgery, rats were fasted, and water was withheld on the day of surgery. Using 7% chloral hydrate, rats were anesthetized via intraperitoneal injection before their skin was disinfected. The rats were then placed on a sterile surgical table and the T12 vertebra (located at the highest point of the spinous process) was identified. Subsequently, we incised the lower back of the rats in the midline, prior to separating the muscles and vertebrae layer-by-layer. The T10-11 SC was completely transected using a blade to induce SCI.

Groupings and Administration

Rats were randomly assigned into six groups (n=6 per group) using a computer-generated random number table to ensure unbiased group distribution: (a) sham-operated, (b) model, (c) low-dose BMSCs treatment (2×10^4 cells/μL), (d) high-dose BMSCs treatment (5×10^4 cells/μL), (e) low-dose Bcl-2-BMSCs treatment (2×10^4 cells/μL), and (f) high-dose Bcl-2-BMSCs treatment groups (5×10^4 cells/μL). The sample size of n=6 per group was chosen based on standard practice in spinal cord injury models and previous studies, ensuring sufficient statistical power for detecting meaningful differences in early recovery outcomes while adhering to ethical considerations regarding animal use.[62] On the first

postoperative day, BMSCs were transplanted in situ in each group. The rats were re-anesthetized and the injured spinal site was re-exposed using the same surgical approach. A cell suspension was prepared at concentrations of 2×10^4 cells/μL and 5×10^4cells/μL for each group, and PBS was used as a blank control. A microinjection syringe was used to inject 5 μL of the BMSCs suspension or PBS into the ventral horn of the SC at the site of injury. The syringe needle was inserted 1.5 mm deep, and after injecting the suspension slowly, the needle was withdrawn slowly prior to keeping it steady for 5 min. The skin and muscles were then sutured in layers. Postoperative care was provided, as described in this study.

Basso, Beattie and Bresnahan (BBB) Score

Based on the existing BBB score,[62] we evaluated open-field motor function on days 0, 3, 14, 21, and 28 post-injuries. Two blind observers, blinded to the group assignments, independently evaluated the locomotor function of each rat. Simultaneous video recordings were made to allow for subsequent verification if needed. To assess the recovery of function after injury and treatment, we employed a BBB score ranging from 0 (no movement of the hind limb) to 21 (normal gait cycle). In addition, the potential of the materials to induce early damage to the normal function of the motor system was determined by conducting BBB testing in animals that were not injured.

Slope tests were performed using a testing apparatus on Days 0, 3, 14, 21, and 28. For each animal, we obtained a single score by averaging the recorded value of the maximal angle at which the rat could maintain its posture without falling for 5 s. All samples were part of separate and independent experiments.

Behavioral Studies

After sciatic nerve injury,[63] several behavioral analyses were conducted on rats, as reported in our earlier study. Evidently, when regeneration of sciatic nerve function was sufficient, we considered this to be the recovery of motor activity in the left hind limb. As described in previous studies,[63,64] locomotion in rats was tracked by analyzing the walking patterns of freely moving rats. During this test, we placed the rats on a track that was 100 mm wide and 500 mm long, while the bottom was covered with white paper, thereby leading to a dark box at the end, and their hind paws were coated with dark dye. The rats were allowed to walk freely, and their gait and locomotion recovery were analyzed.

Histological Observation

Sodium pentobarbital (4 mg/100 g per body weight) was utilized to anesthetize the animals via intra-peritoneal injection after 28 days, which was followed by perfusion with sodium chloride solution (0.9%) and PFA (4%) PBS (0.01M, pH=7.4). Later, we harvested the T8-T10 segments of SC and preserved them in PFA (4%) before embedding them in paraffin. Histopathological evaluations (HE, Nissl, and myelin staining) and subsequent analyses were performed by investigators who were blinded to the experimental groups.

Western Blot Detection of Protein Expression

Using Western blotting, we detected the relative expression of β-tubulin3, MAP2, GFAP, nestin, NF-200, and MBP at protein levels. Proteins were extracted from the SC tissues of the experimental groups using RIPA lysis buffer (Beyotime, Beijing, China). Protein quantification was performed using the BCA protein assay kit according to the manufacturer's instructions and based on the number of standards and samples. Subsequent experimental procedures followed the WB detection method outlined in Effect of Bcl-2 Plasmid-Loaded Cationic Liposomes on BMSCs Differentiation.

Statistical Analysis

All analyses were conducted in GraphPad Prism v8 and R v4.4.1. For each endpoint, we assessed normality of model residuals using the Shapiro–Wilk test and Q-Q plots, and homogeneity of variances using Levene's/Brown–Forsythe tests. When variance heterogeneity was detected, we used Welch's procedures (Welch one-way ANOVA or Welch *t* tests); when normality was doubtful, we used nonparametric alternatives (Mann–Whitney U for two groups; Kruskal–Wallis with Dunn's post-hoc and multiplicity adjustment for ≥3 groups). For the day-28 behavioral outcomes (BBB and inclined plane), we fit a two-way ANOVA with factors Construct (BMSC vs Bcl-2-BMSC) and Dose (Low vs High), including the interaction; planned simple-effects (Construct within each Dose) were Bonferroni-adjusted. We report two-

sided exact *p* values (to three decimals; p<0.001 when smaller) and effect sizes with 95% CIs: Hedges' *g* (small-sample corrected) for pairwise comparisons and η^2/partial η^2 for omnibus effects (95% CIs for partial η^2 obtained in R). Data are shown as mean ± SD. Diagnostic outputs (Shapiro–Wilk, Levene/Brown-Forsythe, Q-Q plots) are provided in Supplementary Figure S1-S2.

Results

Identification of BMSCs

As shown in Figure 1A, third (P3), fourth (P4), and fifth (P5) generations of BMSCs exhibited good growth and were distributed along the bottom of the culture flask. The cells were large and elongated, with bright cytoplasm and good refractive properties, thereby showing minimal variation among them. As shown in Figure 1B, the fluorescent expression of CD34 protein in BMSCs was nearly undetectable, suggesting the minimal presence of CD34 protein in these cells. As illustrated in Figures 1C and D, fluorescence staining revealed high expression levels of CD29 and CD90 in the BMSCs. BMSC identity was confirmed using complementary assays targeting CD29, CD90, and CD34. Flow cytometry demonstrated uniformly high expression of CD29 and CD90 in nearly all cells (≈100% positivity) with minimal CD34 signal (≈1%), consistent with a mesenchymal profile (Figure 1E). Immunofluorescence micrographs showed strong membrane/cytoplasmic staining for CD29 and CD90 and background-level signal in the CD34 channel, while preserving the typical spindle-shaped morphology of cultured BMSCs (Figure 1B–D). The concordance between the quantitative distribution (flow cytometry) and the spatial localization (immunostaining) provided evidence that the isolated cells meet expected MSC marker criteria. Type II collagen (COL2A1) immunostaining was detectable in a subset of baseline (non-induced) cultures (Figure 1F), consistent with chondrogenic marker expression. As shown in Figure 1G, Alizarin Red S staining revealed numerous calcified nodules, which confirmed the differentiation of BMSCs into osteoblasts.

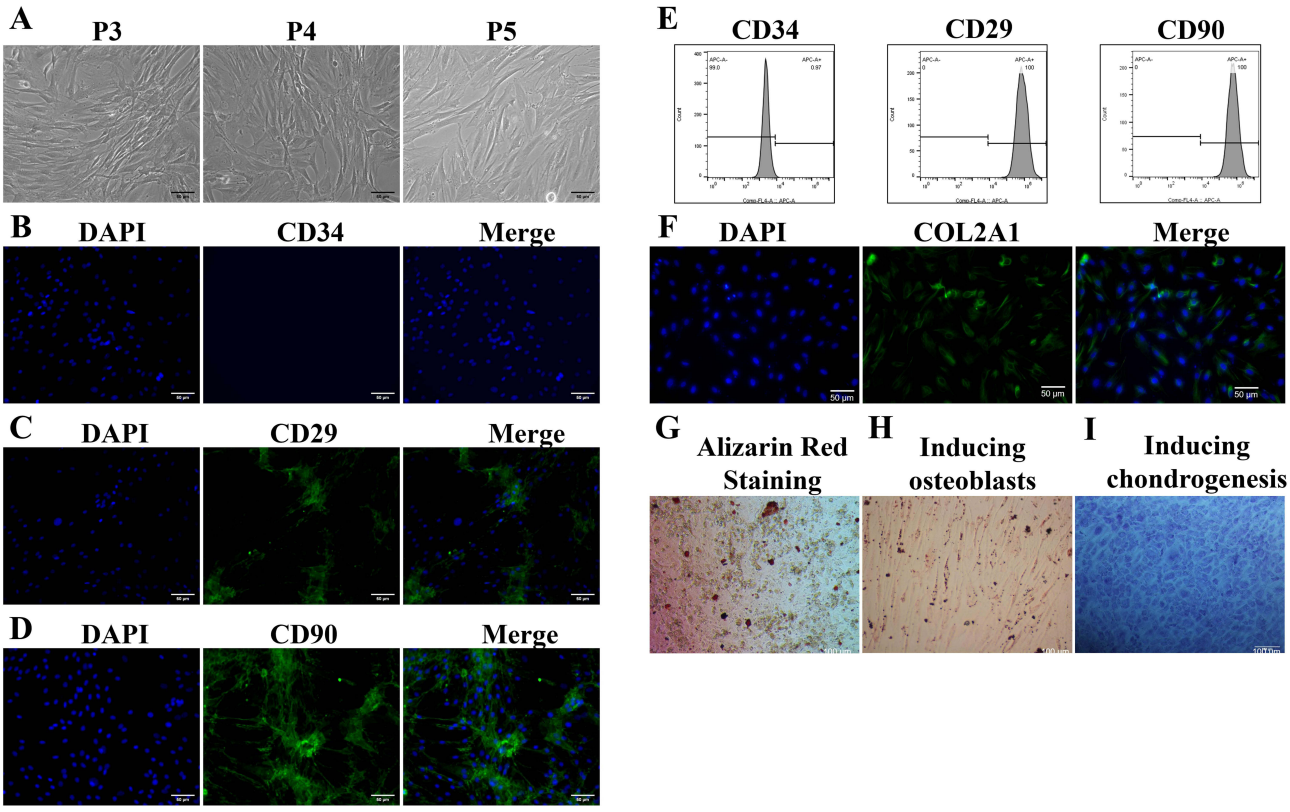

Figure 1 Phenotypic characterization of rat bone marrow mesenchymal stem cells (BMSCs). (**A**) Microscopic images of the cells. (**B**) Fluorescent expression of CD34 protein. (**C**) Fluorescent expression of CD29 protein. (**D**) Fluorescent expression of CD90 protein. (**E**) Flow cytometry results for CD29, CD34, and CD90. (**F**) Immunofluorescence for type II collagen (COL2A1) in baseline culture without chondrogenic induction, shown as a qualitative marker of chondrogenic potential. (**G**) Alizarin Red staining results. (**H**) Oil Red O staining results. (**I**) Toluidine blue staining results. Scale bars: (**B-D, F**) 50 μm; (**G-I**) 100 μm.

https://doi.org/10.2147/DDDT.S513105

Additionally, Figure 1H shows the accumulation of lipid droplets within cells, indicating adipocyte induction. Furthermore, as presented in Figure 1I, Toluidine blue staining displayed abundant proteoglycan deposition, confirming the chondrogenic differentiation of the cells. Collectively, these results confirmed that the cultured cells were BMSCs.

Characterization of Bcl-2 Liposomes

Based on the results in Figures 2A and B, the particle sizes of Blank-liposomes and Bcl-2 liposomes were measured to be 105 ± 1.28 nm and 117 ± 1.75 nm, respectively, with respective PDI of 0.201 ± 0.015 and 0.209 ± 0.017. The zeta potentials were respectively +18.65 ± 1.37 mV and +15.53 ± 1.12 mV. Figures 2C and D illustrate that the TEM results for blank liposomes and Bcl-2 liposomes were consistent with those obtained using the DLS technique, which indicated an average particle size of approximately 100 nm. The liposomes exhibited near-spherical and uniform shapes, with discernible bilayer structures. As depicted in Figure 2E, the content of Rhodamine B in the cells was significantly higher at both 24 and 48 h, which suggests that the cationic liposomes were effectively taken up by BMSCs.

Detection of Cell Viability and Bcl-2 Expression After Transfection of BMSCs

With an increase in the concentrations of Blank-liposome and Bcl-2-liposome, cell viability also decreased gradually (Figure 3A). At a concentration of 100 μg/mL for both Blank-liposome and Bcl-2-liposome, the viability of BMSCs remained above 90%. This level of viability was sufficient to conduct related experiments. Therefore, 100 μg/mL Bcl-2-liposome were chosen for transfection in the subsequent experiments. As shown in Figure 3B, the ELISA results indicated that Bcl-2 protein levels in the control and blank-liposome groups were essentially equivalent, whereas the Bcl-2 protein levels in the Bcl-2-liposome group showed a significant increase compared to the control ($p < 0.01$). This suggests that Bcl-2-liposome effectively facilitated the transfection of Bcl-2 into BMSCs. Similarly, as displayed in Figures 3C and D, Western blot detection results exhibited a trend consistent with those of the ELISA, which further confirms that Bcl-2-liposome efficiently transfected Bcl-2 into BMSCs.

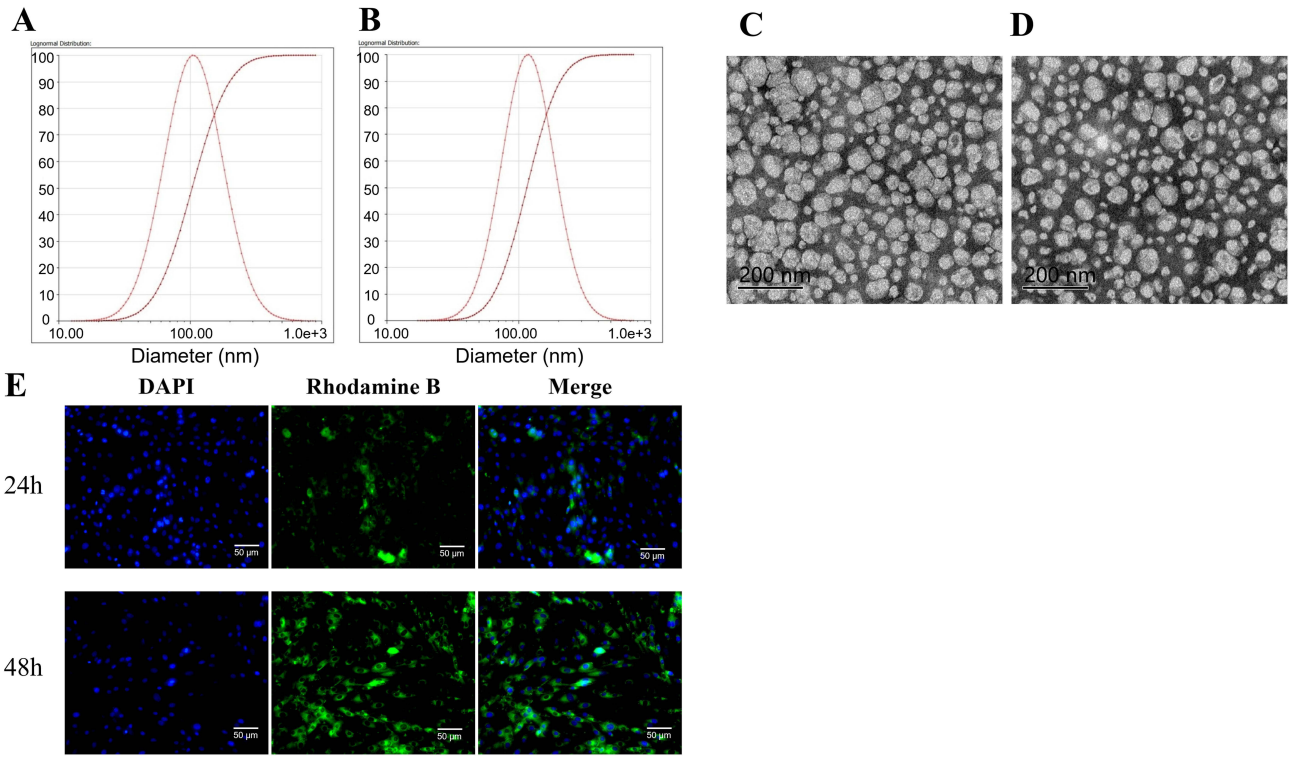

Figure 2 Characterization of Bcl-2 liposomes. (**A**) Particle size of blank liposomes. (**B**) Particle size of Bcl-2 liposomes. (**C**) Transmission electron microscopy (TEM) image of blank liposomes. (**D**) TEM image of Bcl-2 liposomes. (**E**) Results of the uptake capacity analysis of cationic liposomes Scale bars: (**C**–**D**) 200 nm; (**E**) 50 μm.

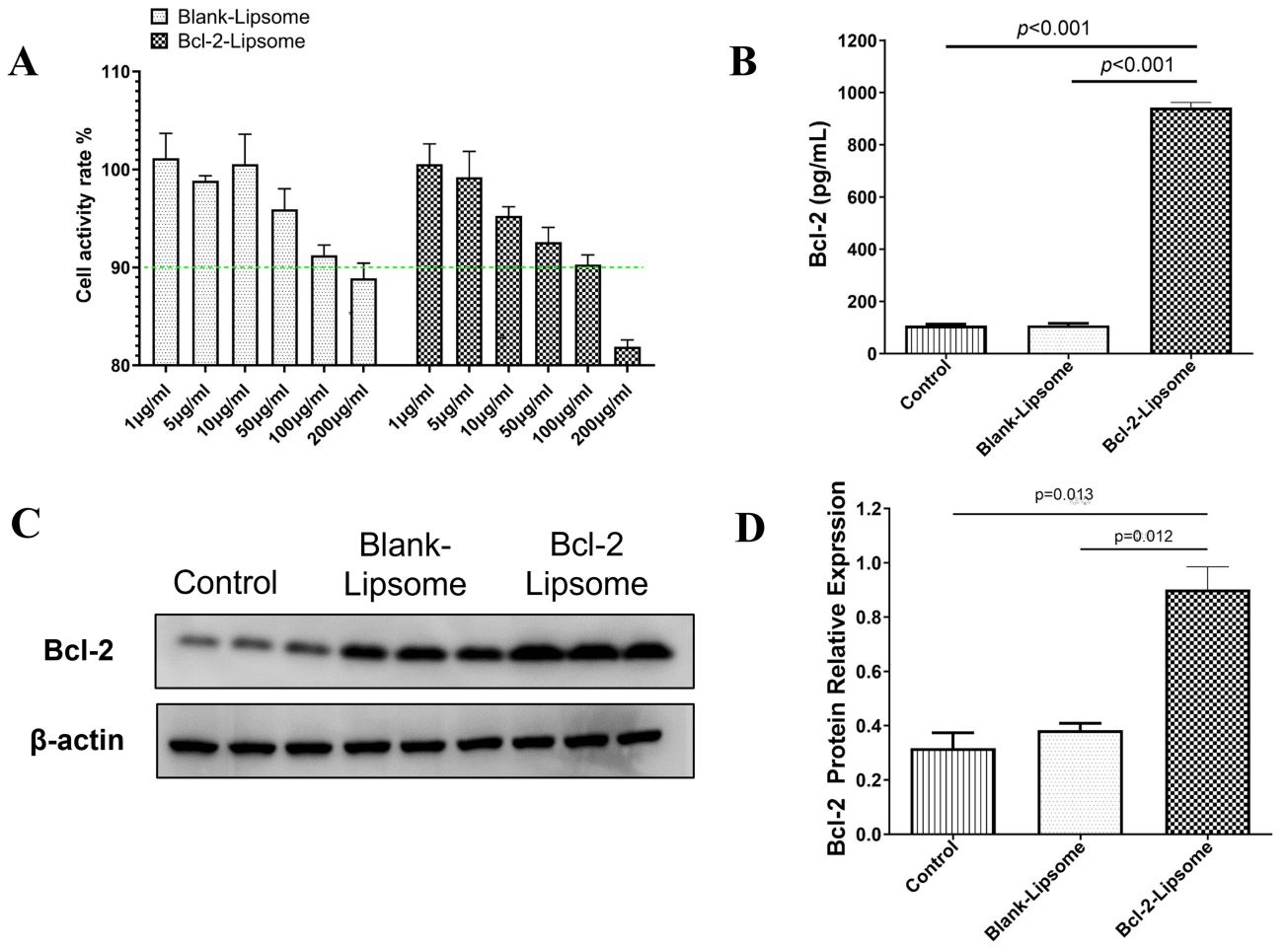

Figure 3 Detection of activity and Bcl-2 expression in transfected rat bone marrow mesenchymal stem cells (BMSCs). (**A**) Activity detection results of BMSCs post-transfection (n=6). (**B**) ELISA for Bcl-2 protein (mean ± SD, n=6). Welch ANOVA: F(2, 9.198)=795.192, p<0.001; fixed-effects η^2=0.995 (95% CI [0.988, 0.997]). Welch pairwise comparisons (Bonferroni-adjusted): Control vs Blank-Liposome p=1.000 (g=−0.10 [−1.15, 0.94]); Control vs Bcl-2-Liposome p<0.001 (g=−21.51 [−30.99, −12.02]); Blank-Liposome vs Bcl-2-Liposome p<0.001 (g=−21.22 [−30.58, −11.86]). Two-sided tests. (**C**) Western blot results for Bcl-2 expression. (**D**) Statistical results of Bcl-2 expression from Western blot (mean ± SD, n=3). β-actin was used as an internal control. One-way ANOVA: $F^{2,6}$=28.339, p<0.001; η^2=0.904 (95% CI [0.860, 0.998]). Pairwise t-tests (Bonferroni-adjusted): Bcl-2-Liposome vs Control t^4=5.791, p_{adj}=0.013 (g=3.78, 95% CI [0.87, 6.70]); Bcl-2-Liposome vs Blank-Lipsome t^4=5.941, p_{adj}=0.012 (g=3.88, 95% CI [0.90, 6.86]). Two-sided tests.

Effects of Bcl-2 Liposomes on Behavioral and Histopathological Outcomes in Rats with SCI

As illustrated in Figure 4A, the BBB score of all rat groups prior to surgery was approximately 20. Following surgery, the scores for the surgical groups dropped to approximately 3 points; however, in the sham-operated group, the scores only decreased to approximately 19 points and quickly recovered. From postoperative weeks 1 to 4, the BBB scores in the SCI group (Group B) remained relatively stable at approximately 3 points, indicating no significant recovery of hind limb motor function. In contrast, the BBB scores of the four treatment groups gradually increased, with the scores for both the high-and low- dose Bcl-2-BMSCs groups exceeding those of the high- and low-dose BMSCs groups (p< 0.01). Notably, the BBB score in the high-dose Bcl-2-BMSCs group (Group F) showed the most significant recovery. This score reached approximately 12 points, which was significantly higher than that of the other groups (p < 0.01), indicating a marked improvement in mobility. Day-28 BBB scores were analyzed with a two-way ANOVA (Construct: Bcl-2-BMSC vs BMSC; Dose: High vs Low). There was a main effect of Construct favoring Bcl-2-BMSCs ($F_{(1,20)}$=4.99, p=0.037; partial η^2=0.20, 95% CI [0.01, 0.55]), whereas the main effect of Dose and the interaction were not significant (Dose: $F_{(1,20)}$ =2.06, p=0.167, partial η^2=0.09; Construct×Dose: $F_{(1,20)}$=0.10, p=0.753, partial η^2=0.01). Planned simple-effects showed

https://doi.org/10.2147/DDDT.S513105

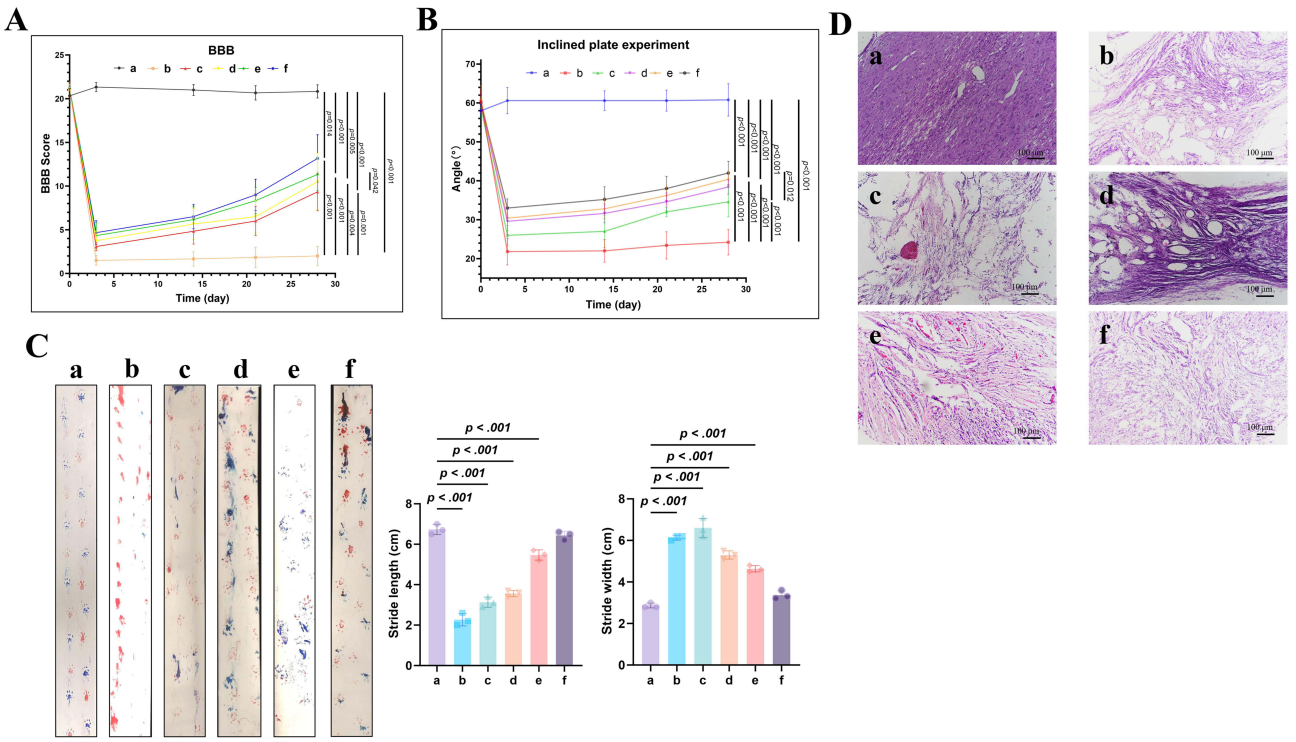

Figure 4 Illustration of the behavioral and pathological examination results of spinal cord (SC) injury (SCI) rats (n=6): (**A**) BBB scores. Two-way ANOVA (Construct: Bcl-2-BMSC vs BMSC; Dose: High vs Low) showed a Construct main effect ($F^{1,20}$=4.99, p=0.037; partial η^2=0.20, 95% CI [0.01, 0.55]); Dose ($F^{1,20}$=2.06, p=0.167; partial η^2=0.09) and Construct×Dose ($F^{1,20}$=0.10, p=0.753; partial η^2=0.01) were not significant. Planned simple-effects (Bonferroni) favored Bcl-2-BMSCs within each dose but did not reach adjusted significance (Low p_{adj}=0.234; High p_{adj} =0.310; g and 95% CIs reported in text). (**B**) Inclined plane test scores. Two-way ANOVA showed a Construct main effect ($F^{1,20}$=11.16, p=0.003; partial η^2=0.36, 95% CI [0.17, 0.64]); Dose ($F^{1,20}$=3.57, p=0.074; partial η^2=0.15) and Construct×Dose ($F^{1,20}$=0.53, p=0.476; partial η^2=0.03) were not significant. Planned simple-effects (Bonferroni) favored Bcl-2-BMSCs at both doses, reaching borderline adjusted significance at Low dose (p_{adj} =0.052; g=1.40, 95% CI [0.75, 2.86]) and trending at High dose (p_{adj} =0.130; g=1.11, 95% CI [0.21, 2.81]). All tests are two-sided. (**C**) Gait analysis. Representative footprint patterns combined with quantitative measurements of stride length and stride width (cm). Quantitative footprint metrics at day 28. Stride length ANOVA (Construct × Dose): $F^{1,8}$=419.59, p<0.001, partial η^2=0.98; Dose: $F^{1,8}$=30.41, p=0.001, partial η^2=0.79; interaction: $F^{1,8}$=4.41, p=0.069. Stride width ANOVA: Construct: $F^{1,8}$=144.09, p<0.001, partial η^2=0.95; Dose: $F^{1,8}$=62.41, p<0.001, partial η^2=0.89; interaction: $F^{1,8}$=0.01, p=0.921. Planned simple-effects (Bcl-2-BMSC vs BMSC): length-Low g=7.42, High g=12.56; width-Low g=−4.61, High g=−7.58 (all p≤0.002); 95% CIs reported in text. (**D**) HE staining results (scale bar: 100 μm). a: sham-operated, b: model, c: low-dose BMSCs treatment (2 × 10^4 cells/μL), d: high-dose BMSCs treatment (5 × 10^4 cells/μL), e: low-dose Bcl-2-BMSCs treatment (2 × 10^4 cells/μL), f: high-dose Bcl-2-BMSCs treatment groups (5 × 10^4 cells/μL).

higher means for Bcl-2-BMSCs within each dose but did not remain significant after adjustment (Low: $t_{(10)}$=1.72, p_{adj} =0.234; g=0.92, 95% CI [0.00, 2.26]. High: $t_{(10)}$=1.54, p_{adj}=0.310; g=0.82, 95% CI [−0.16, 2.40]).

The results of the inclined-plane test are shown in Figure 4B. The preoperative angle for all groups was approximately 58°. Postoperatively, all surgical group angles decreased to approximately 20°, while the angle of the sham-operated group showed minimal change. Furthermore, from week 1 to week 4 post-surgery, the SCI group (Group B) maintained a test angle of approximately 22°, with no notable improvement. Conversely, the angles for the four treatment groups gradually increased, with Bcl-2-BMSC groups again exceeding BMSC groups descriptively. Among them, the high dose Bcl-2-BMSCs group (Group F) exhibited the greatest recovery, with the test angle reaching approximately 37°. At day-28, inclined-plane angles showed a main effect of Construct ($F_{(1,20)}$=11.16, p=0.003; partial η^2=0.36, 95% CI [0.17, 0.64]), indicating Bcl-2-BMSCs outperformed BMSCs when averaging across doses. Dose and the interaction were not significant (Dose: $F_{(1,20)}$=3.57, p=0.074, partial η^2=0.15; Construct×Dose: $F_{(1,20)}$=0.53, p=0.476, partial η^2=0.03). Planned simple-effects favored Bcl-2-BMSCs within each dose, reaching borderline adjusted significance at Low dose ($t_{(10)}$=2.62, p_{adj}=0.052; g=1.40, 95% CI [0.75, 2.86]) and trending at High dose ($t_{(10)}$=2.08, p_{adj}=0.130; g=1.11, 95% CI [0.21, 2.81]).

The footprint analysis results for rats are shown in Figure 4C. Footprints of the sham-operated group were normal, with clear visibility of the toes, whereas the SCI group exhibited almost no footprints of the hind limbs. In contrast, the four treatment groups showed varying degrees of recovery, with the dose Bcl-2-BMSCs group (Group F) demonstrating

the most pronounced effect, as evidenced by clear hind limb footprints, suggesting a degree of restored mobility. Stride length (cm). Two-way ANOVA (Construct × Dose, groups c-f) showed strong main effects of Construct and Dose, with no significant interaction: Construct: $F_{(1,8)}$=419.59, p<0.001, partial η^2=0.98 (95% CI [0.98, 1.00]); Dose: $F_{(1,8)}$=30.41, p=0.001, partial η^2=0.79 (95% CI [0.72, 0.96]); Construct×Dose: $F_{(1,8)}$=4.41, p=0.069, partial η^2=0.36 (95% CI [0.07, 0.82]). Planned simple-effects (Bcl-2-BMSC vs BMSC within dose) were large: Low dose (e vs c): $t_{(4)}$=11.36, p<0.001, g=7.42 (95% CI [5.91, 24.17]); High dose (f vs d): $t_{(4)}$=19.23, p<0.001, g=12.56 (95% CI [11.10, 57.48]). Day-28 (cm): c 3.13±0.25, d 3.57±0.15, e 5.47±0.25, f 6.43±0.21. (For reference: a 6.73±0.25; b 2.27±0.31). Stride width (cm). Two-way ANOVA (Construct × Dose, groups c-f) again showed strong main effects without interaction: Construct: $F_{(1,8)}$=144.09, p<0.001, partial η^2=0.95 (95% CI [0.93, 0.99]); Dose: $F_{(1,8)}$=62.41, p<0.001, partial η^2=0.89 (95% CI [0.85, 0.98]); Construct×Dose: $F_{(1,8)}$=0.01, p=0.921, partial η^2≈0.00 (95% CI [0.00, 0.65]). Simple-effects favored Bcl-2-BMSC (smaller, more normalized widths): Low dose (e vs c): $t_{(4)}$=−7.05, p=0.002, g=−4.61 (95% CI [−32.01, −3.76]); High dose (f vs d): $t_{(4)}$=−11.60, p<0.001, g=−7.58 (95% CI [−36.58, −6.58]). Day-28 means±SD (cm): c 6.60±0.46, d 5.30 ±0.20, e 4.63±0.15, f 3.37±0.21. (For reference: a 2.87±0.12; b 6.13±0.12).

Furthermore, as depicted in Figure 4D, the SC tissue structure in the sham-operated group was compact with no signs of damage. In the SCI model group, SC tissue exhibited significant destruction, with a disorganized structure, sparse chromatin in neurons, fragmented nuclei in some neurons, cell body shrinkage, increased extracellular space, and instances of nuclear disassociation. In the other four treatment groups, the SC tissue showed improvement, particularly in Group F, where the structural integrity of the SC tissue was notably enhanced, with a return to a more normal arrangement and a significant reduction in the extracellular space.

Results of Electron Contrast (EC) and Nissl Staining in SCI Rats

Similar to the insulating layer around electrical wires, the myelin sheath is regarded as a fatty coating that protects the nerve fibers. Electrical impulses are rapidly transmitted between the nerve cells because of the coating. Thus, these electrical signals can be interrupted or halted completely when the myelin is damaged. Demyelination is a common pathological process observed in central nervous system diseases such as SCI; hence, regeneration of myelin around axons is considered a potentially effective strategy to promote functional recovery. The myelin staining kit (modified Page method) utilizes Luxol fast blue (LFB) myelin staining solution to reveal the extent of demyelination, necrosis, and repair under pathological conditions. After staining the SCI sections with myelin, the myelin appeared blue, whereas the demyelinated fibers remained unstained. As shown in Figure 5A, the sham-operated group exhibited a normal cellular structure and precisely arranged neuronal fibers. In the SCI group, significant demyelination and cavitation were observed, indicating myelin damage in the SC of the SCI rats. In all four treatment groups, light blue staining was observed in the damaged areas, with the Bcl-2-BMSc high-dose group displaying the darkest coloration. This observation suggests that Bcl-2-BMSc significantly inhibits white matter demyelination and promotes myelin regeneration.

Nissl staining was used to observe changes in Nissl bodies at the injury site in the SC, thereby assessing neuronal recovery. Following Nissl staining, the neurons appeared purple. As illustrated in Figure 5B, the sham-operated group displayed a distinct purple hue, indicating neurons with normal cellular structures and accurately arranged fibers. In the SCI group, very few purple neurons were observed, accompanied by significant demyelination and cavitation, indicating a high level of neuronal death in the SC of SCI rats. In the four treatment groups, a substantial number of purple neurons were visible in the injured areas, with a significant increase in the neuronal count. Among these, the Bcl-2-BMSc high-dose group exhibited the best results, thereby suggesting its potential to act as a "bridge" at the injury site by connecting the upper and lower nerve fibers and enhancing neuronal survival.

Western Blot Detection Results of SCI Rats

The results of the Western blot (WB) analysis are presented in Figure 6. Compared to the sham surgery group, the relative expression levels of Bcl-2, β-tubulin 3, MAP2, nestin, NF-200, and MBP proteins in the SCI group were significantly reduced, thus showing statistically significant differences. In contrast, the relative expression levels of Bcl-2, β-tubulin 3, MAP2, nestin, NF-200, and MBP proteins increased significantly in all four treatment groups. Notably, the Bcl-2-BMSc high-dose group exhibited the highest relative expression levels of Bcl-2, β-tubulin 3, MAP2, nestin, NF-

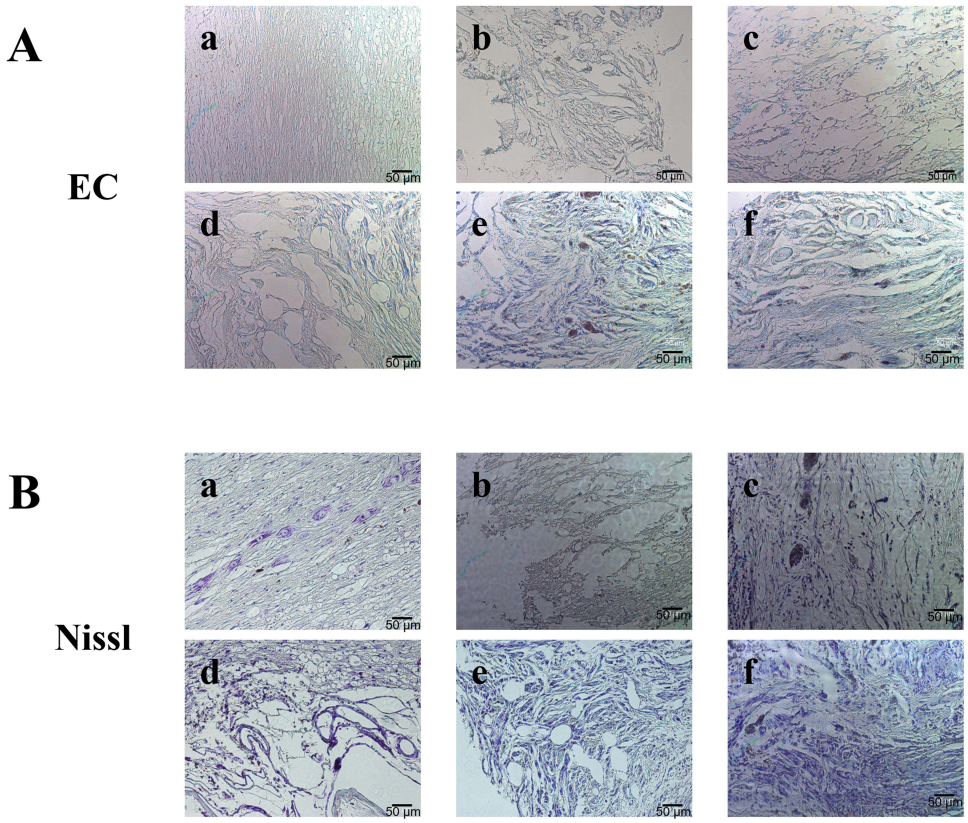

Figure 5 Results of Electron contrast (EC) staining and Nissl staining. (**A**) EC staining results; (**B**) Nissl staining results (Scale bars: 50 μm). a: sham-operated, b: model, c: low-dose BMSCs treatment (2 × 10^4 cells/μL), d: high-dose BMSCs treatment (5 × 10^4 cells/μL), e: low-dose Bcl-2-BMSCs treatment (2 × 10^4 cells/μL), f: high-dose Bcl-2-BMSCs treatment groups (5 × 10^4 cells/μL).

200, and MBP proteins, with significant differences compared with the other groups. Furthermore, the relative expression level of GFAP increased substantially in the SCI group compared to that in the sham-operated group, which is an indication of statistical significance. Conversely, the relative expression levels of GFAP decreased in all four treatment groups, again demonstrating statistically significant differences, with the Bcl-2-BMSc high-dose group exhibiting the lowest relative expression of GFAP.

For the Bcl-2 protein, statistical analysis showed a significant effect for the construct: $F_{(1,8)}$=358.56, p<0.001; partial η^2=0.98 (95% CI [0.97, 1.00]); Dose: $F_{(1,8)}$=11.01, p=0.011; partial η^2=0.58 (95% CI [0.47, 0.91]); Construct×Dose: $F_{(1,8)}$=14.57, p=0.005; partial η^2=0.65 (95% CI [0.49, 0.95]); Simple-effects: Low g=5.38 (95% CI [4.49, 20.03]), $t_{(\approx 4)}$ =8.24, p=0.001; High g=18.69 (95% CI [16.99, 104.94]), $t_{(\approx 4)}$=28.61, p<0.001. For β-tubulin III (neuronal marker), the construct effect was highly significant Construct: $F_{(1,8)}$=1028.56, p<0.001; partial η^2=0.99 (95% CI [0.99, 1.00]); Dose: $F_{(1,8)}$=192.48, p<0.001; partial η^2=0.96 (95% CI [0.95, 0.99]); Construct×Dose: $F_{(1,8)}$=17.00, p=0.003; partial η^2=0.68 (95% CI [0.55, 0.93]); Simple-effects: Low g=12.88 (95% CI [11.24, 39.42]), p<0.001; High g=16.76 (95% CI [15.21, 374.61]), p<0.001. For MAP2 (neuronal dendrites), the construct: $F_{(1,8)}$=453.96, p<0.001; partial η^2=0.98 (95% CI [0.97, 1.00]); Dose: $F_{(1,8)}$=38.13, p<0.001; partial η^2=0.83 (95% CI [0.73, 0.98]); Construct×Dose: $F_{(1,8)}$=10.80, p=0.011; partial η^2=0.57 (95% CI [0.37, 0.89]); Simple-effects: Low g=8.26 (95% CI [7.10, 23.36]), p<0.001; High g=11.45 (95% CI [9.99, 32.02]), p<0.001. GFAP (astroglial) analysis showed a significant construct effect: $F_{(1,8)}$=324.07, p<0.001; partial η^2=0.98 (95% CI [0.96, 1.00]); Dose: $F_{(1,8)}$=10.85, p=0.011; partial η^2=0.58 (95% CI [0.43, 0.92]); Construct×Dose: $F_{(1,8)}$=14.98, p=0.005; partial η^2=0.65 (95% CI [0.54, 0.97]); Simple-effects: Low g=−6.54 (95% CI [−44.48, −5.42]), p<0.001; High g=−10.08 (95% CI [−126.22, −8.36]), p<0.001. For NF-200 (axons), statistical significance was found for the construct: $F_{(1,8)}$=288.20, p<0.001; partial η^2=0.97 (95% CI [0.96, 1.00]); Dose: $F_{(1,8)}$ =52.67, p<0.001; partial η^2=0.87 (95% CI [0.80, 0.98]); Construct×Dose: $F_{(1,8)}$=17.95, p=0.003; partial η^2=0.69 (95% CI

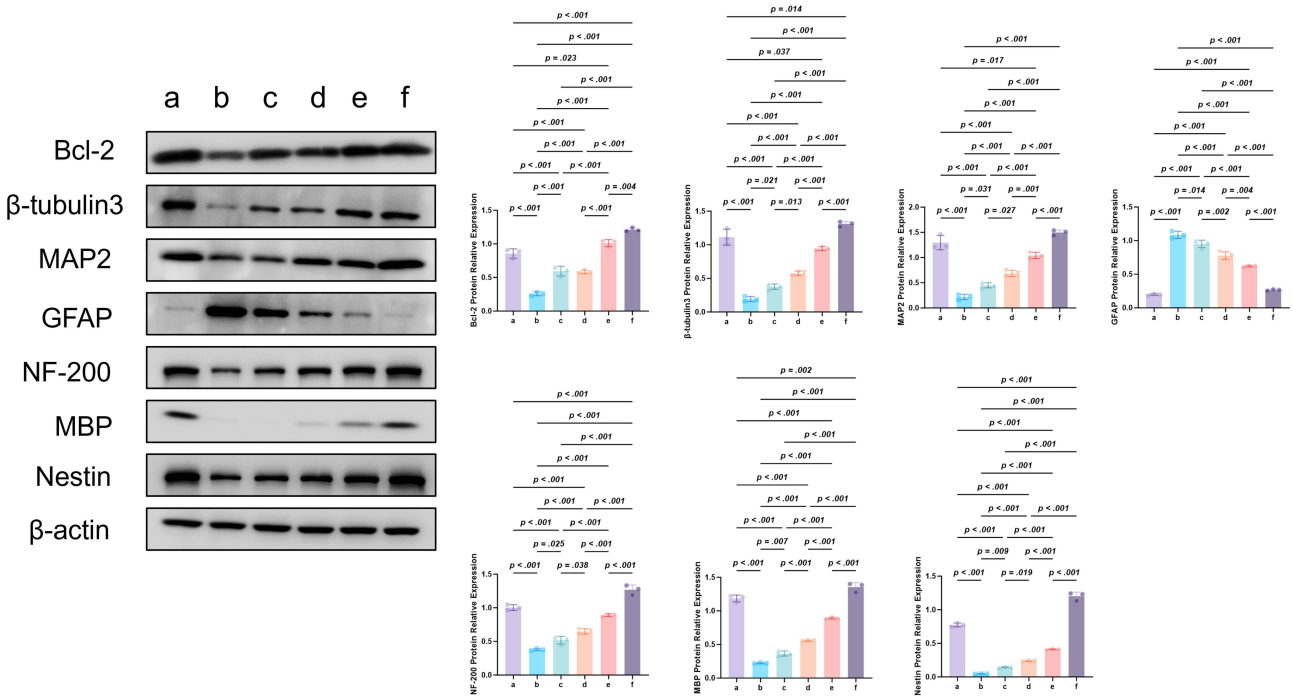

Figure 6 Relative expression levels of Bcl-2, β-tubulin 3, MAP2, GFAP, nestin, NF-200, and MBP proteins as detected by Western blot analysis. β-actin was used as an internal control. Two-way ANOVA (Construct × Dose) on treatment groups (c-f) showed a Construct main effect for all WB markers (partial $\eta^2 \geq 0.95$, all $p<0.001$), with additional Dose effects and select interactions. Planned simple-effects favored Bcl-2-BMSC over BMSC within both doses for each marker (Hedges' g large; 95% CIs reported). For GFAP, effects were negative (lower in Bcl-2-BMSC), consistent with reduced astroglial activation. a: sham-operated, b: model, c: low-dose BMSCs treatment (2×10^4 cells/μL), d: high-dose BMSCs treatment (5×10^4 cells/μL), e: low-dose Bcl-2-BMSCs treatment (2×10^4 cells/μL), f: high-dose Bcl-2-BMSCs treatment groups (5×10^4 cells/μL).

[0.55, 0.96]); Simple-effects: Low g=6.96 (95% CI [6.03, 24.91]), $p<0.001$; High g=8.65 (95% CI [7.41, 57.43]), $p<0.001$. For MBP (myelin), the construct: $F_{(1,8)}=838.01$, $p<0.001$; partial $\eta^2=0.99$ (95% CI [0.99, 1.00]); Dose: $F_{(1,8)}=147.66$, $p<0.001$; partial $\eta^2=0.95$ (95% CI [0.95, 1.00]); Construct×Dose: $F_{(1,8)}=35.60$, $p<0.001$; partial $\eta^2=0.82$ (95% CI [0.74, 0.99]); Simple-effects: Low g=14.82 (95% CI [12.69, 141.31]), $p<0.001$; High g=13.22 (95% CI [11.92, 321.21]), $p<0.001$. Finally, nestin (immature/neuroprogenitor marker) showed a highly significant effect for the construct: $F_{(1,8)}=1192.91$, $p<0.001$; partial $\eta^2=0.99$ (95% CI [0.99, 1.00]); Dose: $F_{(1,8)}=607.00$, $p<0.001$; partial $\eta^2=0.99$ (95% CI [0.98, 1.00]); Construct×Dose: $F_{(1,8)}=385.00$, $p<0.001$; partial $\eta^2=0.98$ (95% CI [0.98, 1.00]); Simple-effects: Low g=26.98 (95% CI [24.15, 141.86]), $p<0.001$; High g=17.98 (95% CI [16.63, 356.52]), $p<0.001$.

Discussion

BMSCs not only possess the advantages of traditional stem cells but have also shown significant potential in areas such as tissue and organ regeneration, studies on functional decline, and treatment of genetic diseases, making them ideal tools for cell and gene therapy.[18,65,66] In this study, we employed density gradient centrifugation and adherence selection to maximize the yield of high-purity cells, while ensuring cell viability. The available literature combines these two methods to isolate and enrich BMSCs from rat bone marrow.[55,67] The obtained BMSCs were identified as high-purity BMSCs using various techniques including immunofluorescence, flow cytometry, Alizarin Red staining, and Oil Red O staining. These techniques have been combined to identify BMSCs in various studies because they are appropriate for the detailed analysis of cell populations and visualization of specific surface markers, which are features of these cells.[68,69] Using both flow cytometry and immunofluorescence strengthens phenotypic validation from complementary angles: flow cytometry quantified population-level marker prevalence with high sensitivity, whereas immunofluorescence confirmed protein localization in the context of cell morphology. The close agreement between methods, including near-universal CD29/CD90 positivity with negligible CD34, supported the assignment of our isolates as bone marrow-derived MSCs and reduced the likelihood that the observed effects arose from hematopoietic contamination. This dual-modality

approach improved internal validity of downstream comparisons by ensuring that treatment effects are evaluated in a well-characterized MSC population.

Transplantation of BMSCs to treat SCI can effectively promote neural functional recovery; however, the ability of BMSCs to directly facilitate axonal regeneration remains controversial.[70,71] Additionally, issues such as low survival and differentiation rates of transplanted BMSCs into neural cells significantly limit their application in SCI.[70,72] Transplantation of BMSCs with elevated Bcl-2 expression yielded robust improvements across astrocytic injury markers, spinal cord tissue pathology, and indices of axonal/synaptic growth,[73] with effects exceeding those observed in control conditions. We implemented a transient, non-viral augmentation by delivering a Bcl-2 expression plasmid to BMSCs using cationic liposome-DNA complexes prior to transplantation. To our knowledge, this is among the first reports that lipoplex-mediated, integration-free Bcl-2 overexpression in BMSCs confers superior day-28 functional outcomes relative to BMSCs alone (Construct main effect on BBB and inclined-plane measures), accompanied by increased Bcl-2 protein and improvements in axonal/myelin readouts. The alignment between behavioral and tissue-level findings, together with the short-term, non-integrating delivery, highlights a practical and scalable route to enhance BMSC therapy for SCI. Given the exploratory sample size, these gains should be validated in larger, prospectively powered studies to refine dose-response and durability, but the present data indicate a clear translational signal.

Construction of a cell vector for the overexpression of Bcl-2 for the treatment of CNS injuries is not a novel approach. As early as 2005, Wei et al transplanted embryonic stem cells (ES cells) overexpressing Bcl-2 into the cerebral cortex of rats with severe focal ischemia.[50] They observed that, after 1–8 weeks post-transplantation, the lesion cavities were filled with cells derived from embryonic stem cells expressing markers for neurons, astrocytes, oligodendrocytes, and endothelial cells.[74] In this study, we adopted a similar approach to fabricate cationic liposomes loaded with Bcl-2 for use in BMSC transplantation.

Cationic liposomes self-assemble from amphiphilic lipids and electrostatically complex plasmid DNA, enabling straightforward, scalable preparation and integration-free, transient expression.[75,76] When appropriately formulated, they exhibit low immunogenicity and acceptable cytotoxicity, and are internalized predominantly via endocytosis with endosomal escape enabling cytosolic/nuclear access. Among non-viral methods (lipid-mediated delivery, electroporation, microinjection, calcium phosphate),[77] cationic lipoplexes offer a practical balance of simplicity and transfection performance across diverse cell types. We did not investigate intracellular trafficking or large-scale manufacturing in this study; both are important for future translation. Beyond these methodological advantages, the present study introduces a novel therapeutic concept by integrating stem cell transplantation with targeted anti-apoptotic gene delivery using this non-viral liposomal system. While BMSCs have been widely investigated for SCI repair, their therapeutic efficacy is often limited by poor survival after transplantation. To address this, we employed cationic liposomes to overexpress Bcl-2 in BMSCs, thereby enhancing cell survival and neuroprotective effects. This dual strategy markedly improved neuronal survival, reduced glial scar formation, and promoted functional recovery, providing a proof-of-concept for a novel regenerative paradigm in SCI therapy. We did not investigate intracellular trafficking or large-scale manufacturing in this study; both are important for future translation.

Our sample size affords adequate sensitivity for large effects at day 28 but limited precision for smaller effects, as reflected by the wide 95% CIs around several estimates. Consequently, non-significant findings for Dose and Construct×Dose should not be taken as evidence of no effect. Larger, prospectively powered studies are warranted to refine these estimates, assess longer-term outcomes, and confirm the observed patterns.

Limitations include the exploratory sample size (n=6/group), which provided adequate sensitivity for large effects but limited power for smaller dose or interaction effects; the focus on a single terminal time point (day 28), which precluded assessment of durability; and a 4-week observation window that did not address long-term safety, although no neoplastic changes were observed here. Quantitative gait was assessed by BBB and inclined plane; footprints were descriptive only. Finally, while the non-viral, integration-free strategy is advantageous, transgene expression is transient, and the optimal balance between expression duration, dose, and safety remains to be defined. Moreover, although our results indicate that Bcl-2 overexpression augments BMSC-mediated repair, the precise molecular mechanisms remain incompletely understood. In vivo tracking of transplanted cells was not performed, thereby limiting insights into their migratory patterns, survival dynamics, and potential synaptic integration within host spinal cord tissue.

Future work should prospectively power multi-dose studies to resolve dose-response and interactions, and extend longitudinal follow-up for durability and safety (including biodistribution and immunogenicity of lipoplexes). We will include mechanistic endpoints to link Bcl-2 expression to circuit repair, for example, apoptosis/survival assays in vivo, electrophysiology, axon tract tracing. Also, combinatorial strategies will explored, for example, rehabilitation, and pro-regenerative cues that might synergize with Bcl-2–augmented BMSCs. Furthermore, the pharmacokinetics, stability, and large-scale manufacturing feasibility of cationic liposomes remain to be systematically characterized. Addressing these aspects, along with the development of standardized protocols for large-scale Bcl-2-BMSC production and rigorous long-term safety testing, will be essential for clinical translation. Additionally, demyelination is a common pathological process observed in central nervous system diseases such as SCI. The myelin sheath, which acts as an insulating layer around nerve fibers, plays a crucial role in the rapid transmission of electrical impulses between nerve cells. Damage to the myelin sheath can lead to disruption or complete halt of these electrical signals. Therefore, regeneration of myelin around axons is considered a potentially effective strategy for promoting functional recovery. This aspect of myelin regeneration is important in the context of SCI repair and should be considered in future therapeutic strategies.

Taken together, our findings indicate a clear translational signal for transient, non-viral Bcl-2 augmentation as a practical means to improve the therapeutic performance of BMSC grafts in SCI, with convergent functional and histological benefits and a favorable short-term safety profile. These data motivate larger, longer-term studies to confirm efficacy, define dosing, and establish durability, and determine whether this combined stem cell–gene therapy strategy can ultimately be advanced as a viable intervention for SCI.

Conclusion

This study explored the application of BMSCs transfected with the Bcl-2 gene via nanogene engineering in the context of SCI in rats, providing preclinical evidence for a potential regenerative strategy to repairing SC damage. The results demonstrated that Bcl-2-transfected BMSCs significantly enhanced neural regeneration, promoted axonal growth, and improved functional recovery compared with controls. These findings are encouraging but should be regarded as proof-of-concept, not definitive evidence, particularly in light of the relatively small sample size and lack of long-term evaluation. Bcl-2 overexpression appears to enhance cell survival and reduce apoptosis, thereby contributing to tissue repair and regeneration in SCI. Nevertheless, further validation in larger animal models and systematic translational studies will be essential. Collectively, this work offers important insights into the potential of combining stem cell therapy with targeted anti-apoptotic gene delivery, while highlighting the need for continued investigation before clinical application.

Acknowledgments

This work was supported by the Wuxi Health Commission Scientific Youth Project (Q202215), Wuxi Health Commission Key Discipline Innovation Team (CXTD2021022), Jiangsu Provincial Health Commission General Project (M2022026) and Wuxi Health Commission Youth Research Project (Q202301).

Disclosure

The authors declared that they do not have any conflicting interest.

References

1. Ahuja CS, Wilson JR, Nori S, et al. Traumatic spinal cord injury. *Nat Rev Dis Primers*. 2017;3(1):17018. doi:10.1038/nrdp.2017.18
2. Spinal Cord Injury (SCI). 2016 Facts and figures at a glance. *J Spinal Cord Med*. 2016;39(4):493–494. doi:10.1080/10790268.2016.1210925
3. Lu Y, Shang Z, Zhang W, et al. Global incidence and characteristics of spinal cord injury since 2000–2021: a systematic review and meta-analysis. *BMC Med*. 2024;22(1):285. doi:10.1186/s12916-024-03514-9
4. Hu X, Xu W, Ren Y, et al. Spinal cord injury: molecular mechanisms and therapeutic interventions. *Signal Transduct Target Ther*. 2023;8(1):245. doi:10.1038/s41392-023-01477-6
5. Anjum A, Yazid MD, Fauzi Daud M, et al. Spinal cord injury: pathophysiology, multimolecular interactions, and underlying recovery mechanisms. *Int J Mol Sci*. 2020;21(20):7533. doi:10.3390/ijms21207533
6. Yang T, Dai Y, Chen G, Cui S. Dissecting the dual role of the glial scar and scar-forming astrocytes in spinal cord injury. *Front Cell Neurosci*. 2020;14.

7. Tran AP, Warren PM, Silver J. New insights into glial scar formation after spinal cord injury. *Cell Tissue Res*. 2022;387(3):319–336. doi:10.1007/s00441-021-03477-w
8. Tian T, Zhang S, Yang M. Recent progress and challenges in the treatment of spinal cord injury. *Protein Cell*. 2023;14(9):635–652. doi:10.1093/procel/pwad003
9. Alvi MA, Pedro KM, Quddusi AI, Fehlings MG. Advances and challenges in spinal cord injury treatments. *J Clin Med*. 2024;13(14):4101. doi:10.3390/jcm13144101
10. Fehlings MG, Wilson JR, Harrop JS, et al. Efficacy and safety of methylprednisolone sodium succinate in acute spinal cord injury: a systematic review. *Global Spine J*. 2017;7(3_suppl):116S–137S. doi:10.1177/2192568217706366
11. Li J, Lepski G, Xu Y-J, Yang F, Lv C-Y, Nie S-M. Cell transplantation for spinal cord injury: a systematic review. *Biomed Res Int*. 2013;2013:1–32. doi:10.1155/2013/729413
12. Jiu J, Liu H, Li D, et al. 3D bioprinting approaches for spinal cord injury repair. *Biofabrication*. 2024;16(3):032003. doi:10.1088/1758-5090/ad3a13
13. Salomonsson SE, Clelland CD. Building CRISPR gene therapies for the central nervous system: a review. *JAMA Neurol*. 2024;81(3):283–290. doi:10.1001/jamaneurol.2023.4983
14. Ma K, Mi CL, Cao XX, Wang TY. Progress of cationic gene delivery reagents for non-viral vector. *Appl Microbiol Biotechnol*. 2021;105(2):525–538. doi:10.1007/s00253-020-11028-6
15. Tian D, You X, Ye J, et al. hBcl2 overexpression in BMSCs enhances resistance to myelin debris-induced apoptosis and facilitates neuroprotection after spinal cord injury in rats. *Sci Rep*. 2024;14(1):1830. doi:10.1038/s41598-024-52167-4
16. Giovannelli L, Bari E, Jommi C, et al. Mesenchymal stem cell secretome and extracellular vesicles for neurodegenerative diseases: risk-benefit profile and next steps for the market access. *Bioact Mater*. 2023;29:16–35. doi:10.1016/j.bioactmat.2023.06.013
17. Demarco FF, de Almeida André D, Nedel F, et al. Stem cells: therapeutic potential in dentistry. *J Contemp Dent Pract*. 2009;10(4):90–96. doi:10.5005/jcdp-10-4-90
18. Hoang DM, Pham PT, Bach TQ, et al. Stem cell-based therapy for human diseases. *Signal Transduct Target Ther*. 2022;7(1):272.
19. Kim N, Cho SG. New strategies for overcoming limitations of mesenchymal stem cell-based immune modulation. *Int J Stem Cells*. 2015;8(1):54–68. doi:10.15283/ijsc.2015.8.1.54
20. Cyranoski D. Canada approves stem cell product. *Nat Biotechnol*. 2012;30(7):571. doi:10.1038/nbt0712-571b
21. Gan L, Liu Y, Cui D, Pan Y, Zheng L, Wan M. Dental tissue-derived human mesenchymal stem cells and their potential in therapeutic application. *Stem Cells Int*. 2020;2020:1–17. doi:10.1155/2020/8864572
22. Sui B, Wu D, Xiang L, Fu Y, Kou X, Shi S. Dental pulp stem cells: from discovery to clinical application. *J Endod*. 2020;46(9):S46–55. doi:10.1016/j.joen.2020.06.027
23. Caplan AI. Adult mesenchymal stem cells for tissue engineering versus regenerative medicine. *J Cell Physiol*. 2007;213(2):341–347. doi:10.1002/jcp.21200
24. Kolf CM, Cho E, Tuan RS. Mesenchymal stromal cells: biology of adult mesenchymal stem cells: regulation of niche, self-renewal and differentiation. *Arthritis Res Ther*. 2007;9(1):204. doi:10.1186/ar2116
25. Mukherjee A, Das B. Mesenchymal stem cells: novel avenues in combating COVID-19. In: *Stem Cells and COVID-19*. Elsevier; 2022:71–94.
26. Matsuzaka Y, Yashiro R. Current strategies and therapeutic applications of mesenchymal stem cell-based drug delivery. *Pharmaceuticals*. 2024;17(6):707. doi:10.3390/ph17060707
27. Xu X, Xu L, Xia J, Wen C, Liang Y, Zhang Y. Harnessing knee joint resident mesenchymal stem cells in cartilage tissue engineering. *Acta Biomater*. 2023;168:372–387. doi:10.1016/j.actbio.2023.07.024
28. Wu S, Sun S, Fu W, Yang Z, Yao H, Zhang Z. The role and prospects of mesenchymal stem cells in skin repair and regeneration. *Biomedicines*. 2024;12(4):743. doi:10.3390/biomedicines12040743
29. Utumi PH, Fracaro L, Senegaglia AC, et al. Canine dental pulp and umbilical cord-derived mesenchymal stem cells as alternative sources for cell therapy in dogs. *Res Vet Sci*. 2021;140:117–124. doi:10.1016/j.rvsc.2021.08.006
30. Costela-Ruiz VJ, Melguizo-Rodríguez L, Bellotti C, et al. Different sources of mesenchymal stem cells for tissue regeneration: a guide to identifying the most favorable one in orthopedics and dentistry applications. *Int J Mol Sci*. 2022;23(11):6356. doi:10.3390/ijms23116356
31. Zhuang WZ, Lin YH, Su LJ, et al. Mesenchymal stem/stromal cell-based therapy: mechanism, systemic safety and biodistribution for precision clinical applications. *J Biomed Sci*. 2021;28(1):28. doi:10.1186/s12929-021-00725-7
32. He Q, Ye Z, Zhou Y, Tan WS. Comparative study of mesenchymal stem cells from rat bone marrow and adipose tissue. *Turkish J Biol*. 2018;42(6):477–489. doi:10.3906/biy-1802-52
33. Bhartiya D, Boheler KR, Rameshwar P. Are mesenchymal cells indeed pluripotent stem cells or just stromal cells? OCT-4 and vsels biology has led to better understanding. *Stem Cells Int*. 2013;2013:1–6. doi:10.1155/2013/813780
34. Zakrzewski W, Dobrzyński M, Szymonowicz M, Rybak Z. Stem cells: past, present, and future. *Stem Cell Res Ther*. 2019;10(1):68. doi:10.1186/s13287-019-1165-5
35. Ding DC, Shyu WC, Lin SZ. Mesenchymal stem cells. *Cell Transplant*. 2011;20(1):5–14. doi:10.3727/096368910X
36. Abbaszadeh H, Ghorbani F, Derakhshani M, et al. Regenerative potential of wharton's jelly-derived mesenchymal stem cells: a new horizon of stem cell therapy. *J Cell Physiol*. 2020;235(12):9230–9240. doi:10.1002/jcp.29810
37. Robert AW, Marcon BH, Dallagiovanna B, Adipogenesis SP. Osteogenesis, and chondrogenesis of human mesenchymal stem/stromal cells: a comparative transcriptome approach. *Front Cell Dev Biol*. 2020;8. doi:10.3389/fcell.2020.00561
38. Kaku M, Akiba Y, Akiyama K, Akita D, Nishimura M. Cell-based bone regeneration for alveolar ridge augmentation – cell source, endogenous cell recruitment and immunomodulatory function. *J Prosthodont Res*. 2015;59(2):96–112. doi:10.1016/j.jpor.2015.02.001
39. Liu S, Schackel T, Weidner N, Puttagunta R. Biomaterial-supported cell transplantation treatments for spinal cord injury: challenges and perspectives. *Front Cell Neurosci*. 2018;11:430.
40. Kadam CY, Abhang SA. Apoptosis Markers in Breast Cancer Therapy. *Advanc Clin Chem*. 2016;74:143–193.
41. Kirkin V, Joos S, Zörnig M. The role of Bcl-2 family members in tumorigenesis. *Biochimica Et Biophysica Acta (BBA)*. 2004;1644(2–3):229–249. doi:10.1016/j.bbamcr.2003.08.009
42. Qian S, Wei Z, Yang W, Huang J, Yang Y, Wang J. The role of BCL-2 family proteins in regulating apoptosis and cancer therapy. *Front Oncol*. 2022;12. doi:10.3389/fonc.2022.985363

43. D'Orsi B, Mateyka J, Prehn JHM. Control of mitochondrial physiology and cell death by the Bcl-2 family proteins Bax and Bok. *Neurochem Int*. 2017;109:162–170. doi:10.1016/j.neuint.2017.03.010
44. Vaux DL, Korsmeyer SJ. Cell death in development. *Cell*. 1999;96(2):245–254. doi:10.1016/S0092-8674(00)80564-4
45. Zhang KZ, Westberg JA, Hölttä E, Andersson LC. BCL2 regulates neural differentiation. *Proc Nat Acad Sci*. 1996;93(9):4504–4508. doi:10.1073/pnas.93.9.4504
46. Mooney R, Majid AA, Mota D, et al. Bcl-2 overexpression improves survival and efficacy of neural stem cell-mediated enzyme prodrug therapy. *Stem Cells Int*. 2018;2018:1–13.
47. Liu W, Yue W, Wu R. Overexpression of Bcl-2 promotes survival and differentiation of neuroepithelial stem cells after transplantation into rat aganglionic colon. *Stem Cell Res Ther*. 2013;4(1):7.
48. Callens M, Kraskovskaya N, Derevtsova K, et al. The role of Bcl-2 proteins in modulating neuronal Ca2+ signaling in health and in Alzheimer's disease. *Biochimica Et Biophysica Acta (BBA)*. 2021;1868(6):118997.
49. Theus MH, Wei L, Cui L, et al. In vitro hypoxic preconditioning of embryonic stem cells as a strategy of promoting cell survival and functional benefits after transplantation into the ischemic rat brain. *Exp Neurol*. 2008;210(2):656–670. doi:10.1016/j.expneurol.2007.12.020
50. Wei L, Cui L, Snider BJ, et al. Transplantation of embryonic stem cells overexpressing Bcl-2 promotes functional recovery after transient cerebral ischemia. *Neurobiol Dis*. 2005;19(1–2):183–193.
51. Jiao J, Huang X, Feit-Leithman RA, et al. Bcl-2 enhances Ca2+ signaling to support the intrinsic regenerative capacity of CNS axons. *EMBO J*. 2005;24(5):1068–1078. doi:10.1038/sj.emboj.7600589
52. Anilkumar U, Prehn JH. Anti-apoptotic BCL-2 family proteins in acute neural injury. *Front Cell Neurosci*. 2014;8:281. doi:10.3389/fncel.2014.00281
53. Wang Y, Sun ZY, Zhang KM, Xu GQ, Li G. Bcl-2 in suppressing neuronal apoptosis after spinal cord injury. *World J Emerg Med*. 2011;2(1):38–44.
54. Mooney R, Majid AA, Mota D, et al. *Bcl-2* overexpression improves survival and efficacy of neural stem cell-mediated enzyme prodrug therapy. *Stem Cells Int*. 2018;2018:7047496. doi:10.1155/2018/7047496
55. Li X, Zhang Y, Qi G. Evaluation of isolation methods and culture conditions for rat bone marrow mesenchymal stem cells. *Cytotechnology*. 2013;65(3):323–334. doi:10.1007/s10616-012-9497-3
56. Song K, Huang M, Shi Q, Du T, Y CAO. Cultivation and identification of rat bone marrow-derived mesenchymal stem cells. *Mol Med Rep*. 2014;10(2):755–760. doi:10.3892/mmr.2014.2264
57. Clabaut A, Grare C, Rolland-Valognes G, et al. Adipocyte-induced transdifferentiation of osteoblasts and its potential role in age-related bone loss. *PLoS One*. 2021;16(1):e0245014. doi:10.1371/journal.pone.0245014
58. Elsana H, Olusanya TOB, Carr-wilkinson J, Darby S, Faheem A, Elkordy AA. Evaluation of novel cationic gene based liposomes with cyclodextrin prepared by thin film hydration and microfluidic systems. *Sci Rep*. 2019;9(1):15120. doi:10.1038/s41598-019-51065-4
59. Elouahabi A, Ruysschaert JM. Formation and intracellular trafficking of lipoplexes and polyplexes. *Mol Ther*. 2005;11(3):336–347. doi:10.1016/j.ymthe.2004.12.006
60. Meisel JW, Gokel GW. A simplified direct lipid mixing lipoplex preparation: comparison of liposomal-, dimethylsulfoxide-, and ethanol-based methods. *Sci Rep*. 2016;6(1):27662. doi:10.1038/srep27662
61. Shah DS, Sakthivel T, Toth I, Florence AT, Wilderspin AF. DNA transfection and transfected cell viability using amphipathic asymmetric dendrimers. *Int J Pharm*. 2000;208(1–2):41–48. doi:10.1016/S0378-5173(00)00534-2
62. Basso DM, Beattie MS, Bresnahan JC. A sensitive and reliable locomotor rating scale for open field testing in rats. *J Neurotrauma*. 1995;12(1):1–21. doi:10.1089/neu.1995.12.1
63. Gu J, Cai X, Raza F, et al. Preparation of a minocycline polymer micelle thermosensitive gel and its application in spinal cord injury. *Nanoscale Adv*. 2024;6(23):5874–5888. doi:10.1039/D4NA00625A
64. Zhang J, Ge H, Li J, et al. Effective regeneration of rat sciatic nerve using nanofibrous scaffolds containing rat ADSCs with controlled release of rhNGF and melatonin molecules for the treatment of peripheral injury model. *Regen Ther*. 2023;24:180–189. doi:10.1016/j.reth.2023.06.009
65. Han Y, Li X, Zhang Y, Han Y, Chang F, Ding J. Mesenchymal stem cells for regenerative medicine. *Cells*. 2019;8(8):886. doi:10.3390/cells8080886
66. Shang F, Yu Y, Liu S, et al. Advancing application of mesenchymal stem cell-based bone tissue regeneration. *Bioact Mater*. 2021;6(3):666–683. doi:10.1016/j.bioactmat.2020.08.014
67. Zhang XQ, Wang L, Zhao SL, Xu W. In vitro cultivation of rat bone marrow mesenchymal stem cells and establishment of pEGFP/Ang-1 transfection method. *Asian Pac J Trop Biomed*. 2014;4(9):701–706. doi:10.12980/APJTB.4.201414B178
68. Li C, Qin T, Zhao J, et al. Bone marrow mesenchymal stem cell-derived exosome-educated macrophages promote functional healing after spinal cord injury. *Front Cell Neurosci*. 2021;15:725573.
69. Luo Z, Sun Y, Qi B, et al. Human bone marrow mesenchymal stem cell-derived extracellular vesicles inhibit shoulder stiffness via let-7a/Tgfbr1 axis. *Bioact Mater*. 2022;17:344–359. doi:10.1016/j.bioactmat.2022.01.016
70. Xia Y, Zhu J, Yang R, Wang H, Li Y, Fu C. Mesenchymal stem cells in the treatment of spinal cord injury: mechanisms, current advances and future challenges. *Front Immunol*. 2023.
71. Zou XF, Zhang BZ, Qian WW, Cheng FM. Bone marrow mesenchymal stem cells in treatment of peripheral nerve injury. *World J Stem Cells*. 2024;16(8):799–810. doi:10.4252/wjsc.v16.i8.799
72. Luo S, Wu J, Qiu Y, et al. Hydrogen promotes the effectiveness of bone mesenchymal stem cell transplantation in rats with spinal cord injury. *Stem Cells Int*. 2023;2023:1–14.
73. Akram R, Anwar H, Javed MS, et al. Axonal regeneration: underlying molecular mechanisms and potential therapeutic targets. *Biomedicines*. 2022;10(12):3186. doi:10.3390/biomedicines10123186
74. Nsairat H, Khater D, Sayed U, Odeh F, Al Bawab A, Alshaer W. Liposomes: structure, composition, types, and clinical applications. *Heliyon*. 2022;8(5):e09394. doi:10.1016/j.heliyon.2022.e09394
75. Khan M. Polymers as efficient non-viral gene delivery vectors: the role of the chemical and physical architecture of macromolecules. *Polymers*. 2024;16(18):2629. doi:10.3390/polym16182629
76. Zhi D, Bai Y, Yang J, et al. A review on cationic lipids with different linkers for gene delivery. *Adv Colloid Interface Sci*. 2018;253:117–140. doi:10.1016/j.cis.2017.12.006
77. Fus-Kujawa A, Prus P, Bajdak-Rusinek K, et al. An overview of methods and tools for transfection of eukaryotic cells in vitro. *Front Bioeng Biotechnol*. 2021;9. 10.3389/fbioe.2021.701031